Optical absorption study by *ab initio* downfolding approach: Application to GaAs

Kazuma Nakamura,[1,*] Yoshihide Yoshimoto,[2] Ryotaro Arita,[3] Shinji Tsuneyuki,[4] and Masatoshi Imada[1,5]
[1]*Department of Applied Physics, University of Tokyo, 7-3-1 Hongo, Bunkyo-ku, Tokyo 113-8656, Japan*
[2]*Institute for Solid State Physics, University of Tokyo, 5-1-5 Kashiwanoha, Kashiwa, Chiba 277-8531, Japan*
[3]*Condensed Matter Theory Laboratory, RIKEN, Wako, Saitama 351-0198, Japan*
[4]*Department of Physics, University of Tokyo, 7-3-1 Hongo, Bunkyo-ku, Tokyo 113-0033, Japan*
[5]*JST, CREST, 7-3-1 Hongo, Bunkyo-ku, Tokyo 113-8656, Japan*
(Received 21 October 2007; revised manuscript received 9 April 2008; published 29 May 2008)

We examine whether the essence and quantitative aspects of electronic excitation spectra are correctly captured by an effective low-energy model constructed from an *ab initio* downfolding scheme. A global electronic structure is first calculated by *ab initio* density-functional calculations with the generalized gradient approximation. With the help of constrained density-functional theory, the low-energy effective Hamiltonian for bands near the Fermi level is constructed by the downfolding procedure in the basis of maximally localized Wannier functions. The excited states of this low-energy effective Hamiltonian ascribed to an extended Hubbard model are calculated by using a low-energy solver. As the solver, we employ the Hartree–Fock approximation supplemented by the single-excitation configuration-interaction method considering electron-hole interactions. The present three-stage method is applied to GaAs, where eight bands are retained in the effective model after the downfolding. The resulting spectra well reproduce the experimental results, which indicate that our downfolding scheme offers a satisfactory framework of the electronic-structure calculation, particularly for the excitations and dynamics as well as for the ground state.

DOI: 10.1103/PhysRevB.77.195126 PACS number(s): 71.35.Cc, 78.20.Bh, 78.40.Fy

I. INTRODUCTION

First-principles electronic-structure calculations based on density-functional theory[1] (DFT) within the local density approximation (LDA) or the generalized gradient approximation (GGA) for the exchange-correlation (XC) functional have opened a way to predict ground-state properties of various materials without introducing *ad hoc* parameters. However, there exist serious problems in which the DFT fails even qualitatively. Typical examples are found in strongly correlated electron systems such as the genuine Mott insulator, where an insulating gap opens in partially filled bands solely owing to the strong local electron-electron repulsion.[2] The DFT with LDA/GGA often predicts metals for these systems,[3] which indicates the fact that the XC functionals based on LDA/GGA do not correctly capture the local correlation in real space. Other typical example is found in dynamics and excitation spectra of electrons, in which many-body correlation effects are also essential.[4,5] Even semiconductors, being supposed to belong to weakly correlated electron systems in the ground state, may have highly degenerate excited states arising from the local electron correlation effects, and thus the single-particle approximations such as the Kohn–Sham[6] (KS) and Hartree–Fock[7] (HF) schemes break down in general. It is well known that incorporating two-particle interactions between electrons and holes generated by the excitation is crucial in describing the electronic structure at low-energy levels. A typical example is found in excitonic excitations.[4,5,8–11]

To properly treat these excitations, we clearly need to go beyond the single-particle theory, while a full *ab initio* calculation taking into account the many-body correlation effects is practically intractable. To go beyond the LDA/Hartree–Fock levels, we are required to develop a sufficiently accurate but efficient and practically feasible method. This challenge, so-called "beyond LDA/Hartree–Fock" problem, has attracted growing interest.[12–21] The GW method[12,13] has been developed to incorporate self-energy effects basically on the level of the random phase approximation (RPA) while strong correlation and fluctuation effects beyond the RPA level require a more accurate and reliable treatment. Especially, an *ab initio* three-stage scheme has been rapidly developed by combining two procedures, namely, LDA/Hartree–Fock framework and accurate low-energy solvers.[15–19] The global electronic structure is first obtained by the LDA/Hartree–Fock scheme. In the next stage, one performs a bridging treatment, that is, *downfolding*,[15,17–19] by eliminating the high-energy degrees of freedom leaving a low-energy effective model (Hamiltonian or Lagrangian) for local bases such as Wannier functions.[22,23] The downfolding determines parameters for the effective low-energy model via first-principles calculations. The resulting low-energy model is, in the final stage, solved by low-energy reliable solvers such as dynamical mean field theory,[15] path-integral renormalization group,[19,24] and/or various Monte Carlo methods[25] developed for treating the correlation effects. Such a hierarchical three-stage scheme instead of a full *ab initio* calculation allows us to perform a first-principles and parameter-free prediction of the electronic structure of the strongly correlated electron system within the present feasibility of computer. The applications of this three-stage scheme to studies of transition-metal oxides such as Sr_2VO_4 and YVO_3 have proven that the scheme really works with high accuracy for the ground-state properties of the strongly correlated electron systems.[15–19] It is, however, by no means trivial whether the downfolded Hamiltonian extracted from the same procedure correctly describes excitation spectra and dynamics. The crucial and highly nontrivial point to be examined is whether the low-energy effective Hamiltonian ex-

tracted from the downfolding procedure gives a legitimate and quantitatively accurate starting point for the understanding of the excitation spectra.

In this paper, we present theoretical studies on the *ab initio* downfolding scheme to assess the reliability for treating dynamical properties. In our scheme, maximally localized Wannier functions (MLWFs) are introduced as a basis function for representing the model Hamiltonian. This basis offers a computationally convenient choice, because this Wannier function can be computed with any basis functions (plane wave,[22] linearized muffin-tin orbital,[26] linearized augmented plane wave,[27] etc). Transfer parameters are evaluated by calculating Kohn–Sham matrix elements in this basis, and on-site and/or off-site interaction parameters including screening effects are determined via constrained calculations.[16–18,28,29]

In the three-stage scheme, the reliability of the downfolding procedure and the accuracy of the resulting model parameters are crucially important. In particular, the reliability in describing dynamics and excitation spectra has to be critically tested. For this purpose, we make a critical comparison between experimental results and computational results for the generated model. In the present study, we focus on optical absorption properties. It is widely recognized and accepted in literature that the optical absorption of solids, in particular, for semiconductors or insulators, is deeply affected by excitonic effects.[4,5] This effect originates from an effective Coulomb interaction between electrons and holes and therefore is sensitive to the magnitude of the interaction parameters in the model Hamiltonian. To examine this effect through the present formalism, we choose GaAs as a representative material exhibiting spectral enhancement due to the excitonic effect or more specifically the coupling of the electron-hole configurations[10] and calculate its optical spectra by taking account of the electron-hole interaction. There exist many experimental[30,31] and highly accurate *ab initio*[10,11] spectral data for this material. Therefore, our downfolding formalism and determined parameters can be critically tested by examining whether our model spectrum satisfactorily reproduces those data.

This paper is organized as follows: In Sec. II, we describe our downfolding procedure; we introduce a complete-neglect-differential-overlap (CNDO) model, which is used as our target model Hamiltonian and describe computational details for determining the model parameters. In Sec. III, to take into account the electron-hole interaction, we introduce a single-excitation (SE) configuration-interaction (CI) framework for calculating an optical absorption. Efficient techniques to evaluate one-body velocity matrix elements needed in the spectral calculation, based on the Wannier interpolation scheme, are described in Appendixes A and B. The calculated optical spectra are compared to the experimental results. Concluding remarks are given in Sec. IV.

II. DOWNFOLDING PROCEDURE

A. Global electronic structure by density-functional theory

The first procedure derives the global electronic band structure by a conventional DFT scheme. The present scheme is based on *ab initio* density-functional calculations with Tokyo *ab initio* program package[32] developed by the condensed-matter-theory group in the University of Tokyo. With this code, band calculations have been performed within the generalized gradient approximation[33] to the exchange correlation functional, using a plane-wave basis set and the Troullier–Martins norm-conserving pseudopotentials[34] in the Kleinman–Bylander representation.[35] The energy cutoff is set to 25 Ry, and a $15\times15\times15$ k-point sampling is employed to represent electronic structures of the system. The resulting global band structure of GaAs at an energy region [−15 eV: +30 eV] is illustrated in the left panel of Fig. 1.

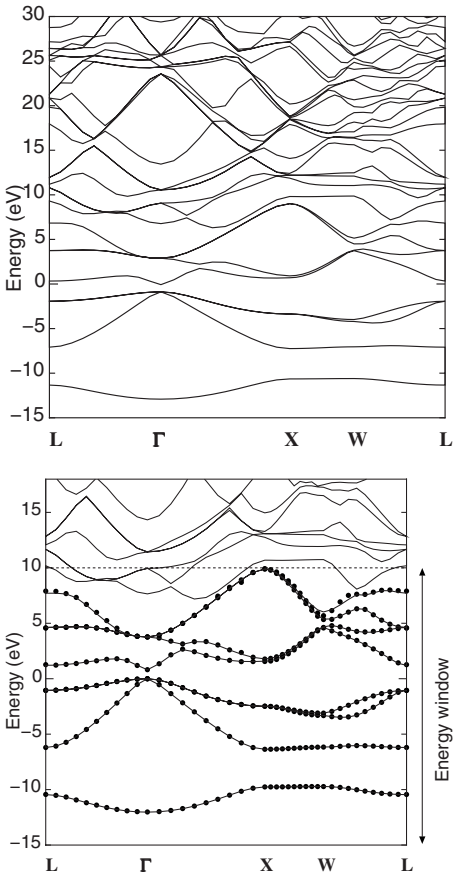

FIG. 1. (Top) A global *ab initio* band structure of GaAs at [−15 eV:+30 eV]. (Bottom) *Ab initio* original (solid line) and interpolated (dots) bands. Energy zero is set to the top of the valence bands. The energy window is set to [−15 eV:+10 eV].

B. Complete-neglect-differential-overlap model

Now, we go onto the second stage and start the derivation of an effective low-energy Hamiltonian by the downfolding procedure. Before going to the downfolding itself, we first specify the form of the final effective low-energy Hamiltonian. In the present downfolding procedure, we will make several approximations by simplifying the low-energy effective Hamiltonian, in which we expect that the approximations do not seriously alter the optical spectra. The first approximation is to consider only the diagonal Coulomb

interaction and ignore the off-diagonal part (exchange interaction) in the low-energy effective model, which results in an extended Hubbard model or, in other words, the CNDO model. The CNDO Hamiltonian has originally been introduced by Pople *et al.*[36] to study electronic structures of small organic molecules and, to date, has been extended to study various properties of complicated systems ranging from transition-metal compounds[37] to proteins[38] and DNA.[39] A remarkable property of this Hamiltonian is that it considers all the degrees of freedom of valence electrons of the system, which allows describing the individual characters of the real material.

The crystal CNDO Hamiltonian $\mathcal{H}$ consists of a one-body part $\mathcal{H}_t$ and an interaction part $\mathcal{H}_C$ as follows:

$$\mathcal{H} = \mathcal{H}_t + \mathcal{H}_C. \tag{1}$$

The one-body part $\mathcal{H}_t$ is given by

$$\mathcal{H}_t = \sum_{\sigma} \left\{ \sum_{\boldsymbol{R}} \sum_{i} \sum_{\mu} I_{\mu i} a^{\sigma\dagger}_{\mu i \boldsymbol{R}} a^{\sigma}_{\mu i \boldsymbol{R}} + \sum_{\boldsymbol{R}\boldsymbol{R}'} \sum_{ij} \sum_{\mu\nu} t_{\mu i \nu j}(\boldsymbol{R}' - \boldsymbol{R}) a^{\sigma\dagger}_{\mu i \mathbf{R}} a^{\sigma}_{\nu j \boldsymbol{R}'} \right\}, \tag{2}$$

where $a^{\sigma\dagger}_{\mu i \boldsymbol{R}}$ ($a^{\sigma}_{\mu i \boldsymbol{R}}$) is a creation (annihilation) operator of a valence electron with spin σ in μ-type localized basis centered at the ith site in lattice $\boldsymbol{R}$. As mentioned in Sec. I, we use the MLWF as the basis function for representing the CNDO Hamiltonian. In the present study of GaAs, there are eight WFs in the primitive cell, where the first four belong to a Ga site, and the remaining four belong to an As site. Thus, the index μ specifies four types of lobe directions (band indices) of the MLWFs, and the suffix i specifies the Ga or As sites. $I_{\mu i}$ and $t_{\mu i \nu j}(\boldsymbol{R}-\boldsymbol{R}')$ are the ionization potential and the transfer integral, respectively. Notice that the translational symmetry in the crystal is explicitly considered for matrix elements; $I_{\mu i \boldsymbol{R}} = I_{\mu i}$ and $t_{\mu i \boldsymbol{R} \nu j \boldsymbol{R}'} = t_{\mu i \nu j}(\boldsymbol{R}' - \boldsymbol{R})$ for any $\boldsymbol{R}$ and $\boldsymbol{R}'$.

The interaction part $\mathcal{H}_C$ is written as

$$\mathcal{H}_C = \sum_{\boldsymbol{R}} \left\{ \sum_{i} \sum_{\mu} U_i N^{\uparrow}_{\mu i \boldsymbol{R}} N^{\downarrow}_{\mu i \boldsymbol{R}} + \sum_{i} \sum_{\mu<\nu} U'_i N_{\mu i \boldsymbol{R}} N_{\nu i \boldsymbol{R}} \right\} + \sum_{\boldsymbol{R}\boldsymbol{R}'} \sum_{ij} V_{ij}(\boldsymbol{R} - \boldsymbol{R}')(N_{i\boldsymbol{R}} - Z_i)(N_{j\boldsymbol{R}'} - Z_j). \tag{3}$$

Here, $N^{\sigma}_{\mu i \boldsymbol{R}} = a^{\sigma\dagger}_{\mu i \boldsymbol{R}} a^{\sigma}_{\mu i \boldsymbol{R}}$, $N_{\mu i \boldsymbol{R}} = \Sigma_{\sigma} N^{\sigma}_{\mu i \boldsymbol{R}}$, and $N_{i\boldsymbol{R}} = \Sigma_{\mu} N_{\mu i \boldsymbol{R}}$ are the number operators, and Z_i is the core charge. U_i and U'_i are the on-site intraorbital and interorbital Coulomb repulsions, respectively. $V_{ij}(\boldsymbol{R}-\boldsymbol{R}')$ in the third term is an interatomic Coulomb repulsion, and it is assumed to be independent of the lobe directions μ and ν.

C. Parametrization

We now describe the downfolding procedure and parametrization for the CNDO model of Eq. (1). The downfolding consists of two parts. The first is the derivation of the kinetic energy part, where a tight-binding Hamiltonian $\mathcal{H}_t$ is derived. The second part is the derivation of the interaction part $\mathcal{H}_C$.

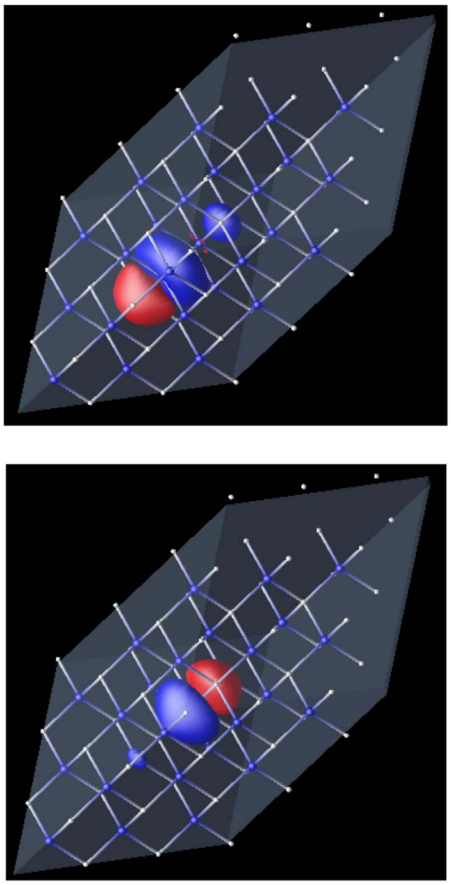

FIG. 2. (Color online) Maximally localized Wannier functions of Ga (top) and As (bottom). The amplitudes of the contour surface are $+0.5/\sqrt{v}$ (dark shaded balls) and $-0.5/\sqrt{v}$ (lightly shaded balls), where v is the volume of the primitive cell. The shaded sheet represents a $3\times3\times3$ fcc lattice and Ga and As nuclei are illustrated as gray and blue dots.

1. Kinetic energy

The tight-binding Hamiltonian $\mathcal{H}_t$ given in Eq. (2) is derived from the global band structure after eliminating higher-energy bands. This downfolding may be performed by the perturbation scheme.[17–19] The resultant band structure is normally very close to the low-energy part of the original band structure and the difference is not discernible when the low-energy retained part is isolated from the eliminated high-energy bands.[17–19] This means that the self-energy of the retained bands caused by the higher-energy eliminated electrons is negligible. Since such self-energy effects are smaller even in semiconductor systems, in this paper, we employ the low-energy part of the bands as the retained bands after the elimination of the higher-energy bands.

Now, we retain eight bands near the Fermi level and construct Wannier orbitals from the retained band structure. To this end, *ab initio* MLWFs are constructed with the Souza–Marzari–Vanderbilt algorithm.[22] We set an energy window in the interval [−15 eV: +10 eV], which includes four valence and four conduction bands of the system. The resulting Ga and As MLWFs are displayed in the left and right panels of Fig. 2, respectively. We see that the Wannier functions are

almost localized at a single site and have an anisotropic character due to an sp^3 hybridization. To show the accuracy of low-energy band structures represented by the resultant WFs, we compare in the right panel of Fig. 1 original bands (solid line) to interpolated bands (dots) obtained by diagonalizing k-space KS Hamiltonian matrices represented by the WFs. We see a good agreement between the original and interpolated bands in the energy window. Ionization potential $I_{\mu i}$ and transfer integral $t_{\mu i \nu j}(\boldsymbol{R})$ are extracted from the matrix elements of the one-body KS Hamiltonian $\hat{h}_{\mathrm{KS}}$ in the basis of the MLWFs $|w_{\mu i \boldsymbol{R}}\rangle$ as

$$I_{\mu i} = \langle w_{\mu i \boldsymbol{0}} | \hat{h}_{\mathrm{KS}} | w_{\mu i \boldsymbol{0}} \rangle \quad \text{and} \quad t_{\mu i \nu j}(\boldsymbol{R}) = \langle w_{\mu i \boldsymbol{0}} | \hat{h}_{\mathrm{KS}} | w_{\nu j \boldsymbol{R}} \rangle, \tag{4}$$

respectively. Here, $\boldsymbol{R} = l\boldsymbol{a}_1 + m\boldsymbol{a}_2 + n\boldsymbol{a}_3$ with $-7 \leq (l,m,n) \leq +7$, and $\{\boldsymbol{a}_1, \boldsymbol{a}_2, \boldsymbol{a}_3\}$ are primitive lattice vectors.

2. Interaction energy

We next derive the interaction parameters U_i, U_i', and $V_{ij}(\boldsymbol{R})$ for the low-energy model. In the original CNDO framework, the Coulomb interaction between electrons has a long-range tail as scaled by $1/r$ in the limit $r \to \infty$ with r being a distance between two electrons. We are, however, interested in the electronic interaction in condensed phase for which the Coulomb interaction is effectively screened. In fact, the dielectric constant of GaAs is rather high; $\epsilon_0 = 10.6$ experimentally,[40] which indicates that the Coulomb interaction decays as $1/(\epsilon_0 r)$ in the limit $r \to \infty$. We thus employ an approximation for this interaction; we keep only on-site interactions U_i and U_i' and the nearest-neighbor interaction V.

These parameters are determined with a constrained DFT framework following a "hopping-cutoff" treatment.[41] As the basic strategy, one first kinetically decouple a specific site from the rest of the system, thus leaving this site isolated as the so-called atomic limit. This decoupling treatment is achieved by switching off the hoppings between the Wannier orbitals at the specific site and all the other orbitals, where we identify the hoppings with the off-diagonal Kohn–Sham matrix elements in the representation of the Wannier functions. With such a hopping cutoff, the standard constrained total-energy calculations are performed to generate a potential-energy surface with respect to constrained parameters such as occupancies of the Wannier orbitals belonging to the decoupled site. The interaction parameters obtained with quadratic fitting to the resulting potential-energy data include screening effects ascribed to the relaxation of the valence electron density around the decoupled site. In the present case, the procedure for determining the interaction parameters is somewhat complicated because of a large number of the interaction parameters to be derived. So, in the practical work, we divide the treatment into two steps: the determination of U and U' and the subsequent step for determining an off-site parameter V.

The basic strategy for obtaining U and U' is to generate potential-energy-data sets with respect to two types of the constrained parameters: (I) the first potential-energy data are obtained from the constrained calculations with respect to occupancy $q_{\mu I}$ of a specific Wannier orbital μ at the site I, and (II) another data are obtained from the constrained calculations for a site occupancy Q_I defined as the total amount of the orbital occupancies belonging to this site, $\Sigma_\mu q_{\mu I}$. The curvature of the first potential-energy curve plotted as a function of the orbital occupation $q_{\mu I}$ gives an estimate of the on-site intraorbital interaction for the orbital μ at the site I, while the curvature of the second data represents the averaged value over the on-site intraorbital and/or interorbital interactions. From quadratic fitting to the mixed two data, we can reasonably determine the U and U' parameters (see below). Although the types of the constraints are different in the two calculations, the method itself is the same, so, here, we describe only details for the constrained calculation with respect to the single orbital occupancy.

The practical calculation proceeds as follows: We first consider a $3 \times 3 \times 3$ fcc supercell containing 54 atoms,[42] and choose the central Ga site placed at the origin as the decoupled site. (Here, we describe only the Ga case, but a parallel treatment can be applied to the U and U' determination for the As site.) We next introduce a cutting operator $\hat{\Lambda}_{\mathrm{cut}}$ to switch off the hopping integrals connecting the four Wannier orbitals of this site to the other Wannier orbitals,

$$\hat{\Lambda}_{\mathrm{cut}} = -\hat{P}_{I\boldsymbol{0}} \hat{h}_{\mathrm{KS}} \hat{P}_W - \hat{P}_W \hat{h}_{\mathrm{KS}} \hat{P}_{I\boldsymbol{0}} + \hat{P}_{I\boldsymbol{0}} \hat{h}_{\mathrm{KS}} \hat{P}_{I\boldsymbol{0}} + \sum_\mu |w_{\mu I \boldsymbol{0}}\rangle I_{\mu I} \langle w_{\mu I \boldsymbol{0}}|, \tag{5}$$

where $\hat{h}_{\mathrm{KS}}$ is a one-body KS Hamiltonian, and $\hat{P}_W$ is a projector onto the total Wannier orbitals,

$$\hat{P}_W = \sum_{\boldsymbol{X}} \sum_i \sum_\mu |w_{\mu i \boldsymbol{X}}\rangle \langle w_{\mu i \boldsymbol{X}}|. \tag{6}$$

Here, $\boldsymbol{X}$ is a lattice vector denoting a supercell, the suffix i specifies the sites in the supercell, and μ stands for the band index of the Wannier orbital. $\hat{P}_{I\boldsymbol{0}}$ in Eq. (5) is a projector onto the Wannier orbitals belonging to the decoupled I site in the home cell ($\boldsymbol{X} = \boldsymbol{0}$) ,

$$\hat{P}_{I\boldsymbol{0}} = \sum_\mu |w_{\mu I \boldsymbol{0}}\rangle \langle w_{\mu I \boldsymbol{0}}|. \tag{7}$$

With the cutting operator in Eq. (5), we define the constrained total energy as

$$E_{\mathrm{ctot}} = \min_\rho \left\{ \mathcal{F}[\rho] + \frac{1}{N} \sum_{\boldsymbol{k}} \sum_\alpha f_{\alpha \boldsymbol{k}} \langle \phi_{\alpha \boldsymbol{k}} | \hat{\Lambda}_{\mathrm{cut}} | \phi_{\alpha \boldsymbol{k}} \rangle + \lambda_{\mu I \boldsymbol{0}} \left[\frac{1}{N} \sum_{\boldsymbol{k}} \sum_\alpha f_{\alpha \boldsymbol{k}} |\langle w_{\mu I \boldsymbol{0}} | \phi_{\alpha \boldsymbol{k}} \rangle|^2 - q_{\mu I \boldsymbol{0}} \right] \right\}. \tag{8}$$

Here, $\mathcal{F}[\rho]$ is a usual density functional with a total charge density $\rho(\boldsymbol{r}) = \frac{1}{N} \Sigma_{\alpha \boldsymbol{k}} f_{\alpha \boldsymbol{k}} |\phi_{\alpha \boldsymbol{k}}(\boldsymbol{r})|^2$ with N being the total number of k points, the first term in the bracket $[\cdots]$ is the definition itself for the orbital occupancy of the disconnected Wannier orbital $|w_{\mu I \boldsymbol{0}}\rangle$, and $\lambda_{\mu I \boldsymbol{0}}$ is the Lagrange multiplier associated with the constraint to fix the orbital occupancy at $q_{\mu I \boldsymbol{0}}$. A functional derivative of E_{ctot} with respect to the Bloch orbital $\phi_{\alpha \boldsymbol{k}}$ leads to the following constrained KS equation:

$$[\hat{h}_{\mathrm{KS}} + \hat{\Lambda}_{\mathrm{cut}} + \lambda_{\mu I\mathbf{0}}|w_{\mu I\mathbf{0}}\rangle\langle w_{\mu I\mathbf{0}}|]|\phi_{\alpha\mathbf{k}}\rangle = \epsilon_{\alpha\mathbf{k}}|\phi_{\alpha\mathbf{k}}\rangle, \quad (9)$$

where the third term in the left hand side is an additional potential due to the occupancy constraint. For numerical details for solving the equation, readers are referred to Ref. 43. By solving the equation, we generate constrained potential-energy data (we refer to these data as DATA I), and plot them as functions of the orbital occupancy $q_{\mu I\mathbf{0}}$ and the site occupancy $Q_{I\mathbf{0}}=\Sigma_\mu q_{\mu I\mathbf{0}}$. In parallel to this treatment, the constrained calculations for the site occupancy are performed, where there is a small modification in the constrained KS equation (9); the additional potential is changed to $\lambda_{I\mathbf{0}}\Sigma_\mu|w_{\mu I\mathbf{0}}\rangle\langle w_{\mu I\mathbf{0}}|$. We again monitor the calculated constrained total energies as functions of $q_{\mu I\mathbf{0}}$ and $Q_{I\mathbf{0}}$ (DATA II). With the resulting DATA I and II, we perform quadratic fitting of the following function around $q_{\mu I\mathbf{0}}=\bar{q}_{\mu I\mathbf{0}}$ and $Q_{I\mathbf{0}}=\bar{Q}_{I\mathbf{0}}$:

$$f(Q_{I\mathbf{0}}, q_{\mu I\mathbf{0}}) = \tfrac{1}{2}U_{\mathrm{Ga}}(Q_{I\mathbf{0}} - \bar{Q}_{I\mathbf{0}})^2 + 2(U'_{\mathrm{Ga}} - U_{\mathrm{Ga}})(Q_{I\mathbf{0}} - \bar{Q}_{I\mathbf{0}}) \times (q_{\mu I\mathbf{0}} - \bar{q}_{\mu I\mathbf{0}}) + 2(U_{\mathrm{Ga}} - U'_{\mathrm{Ga}})(q_{\mu I\mathbf{0}} - \bar{q}_{\mu I\mathbf{0}})^2, \quad (10)$$

where $\bar{q}_{\mu I\mathbf{0}}$ and $\bar{Q}_{I\mathbf{0}}$ are equilibrium occupancies taken from the global band structure with no additional potential ($\lambda_{\mu I\mathbf{0}}=0$). The form of the fitting function in Eq. (10) is derived by exploiting the character of the fourfold degeneracy of the Wannier orbitals $\{w_{\mu I\mathbf{0}}\}$ (Appendix A). The U_{Ga} and U'_{Ga} values thus obtained are 2.39 and 2.17 eV, respectively, which are largely reduced from the bare interaction values $U^0_{\mathrm{Ga}}=9.25$ eV and $U'^0_{\mathrm{Ga}}=7.89$ eV. The same procedure is applied to the U and U' determinations of the As site. It was found to be $U_{\mathrm{As}}=2.71$ eV and $U'_{\mathrm{As}}=2.09$ eV. The corresponding bare values U^0_{As} and U'^0_{As} are 11.45 and 9.80 eV, respectively.

We next describe the determination of the off-site parameter V. The interaction depends on the relative configuration between the Wannier orbitals. For example, let us consider a configuration formed by a pair of the Ga Wannier orbital and the As Wannier orbital, where these orbitals face along the covalent bond of the two atoms (we call it *facing configuration*). An example for the facing configuration can be found in the two Wannier orbitals displayed in the left and right panels of Fig. 2. Obviously, the strength of the Coulomb repulsion in the facing configuration is relatively large compared to that in the other configurations. It should be noted here that the V parameter affects *renormalized* transfer integrals [see Eq. (12) in Sec. II D for the explicit form of the renormalized transfer integral]. Since bonding and antibonding orbitals are formed by the Wannier orbitals in the facing configuration, the bonding and antibonding splitting, i.e., band gap itself, is dominated by the magnitude of a renormalized transfer integral between the Wannier orbitals in the facing configuration. Thus, the V value in this configuration is crucial for an accurate description of the low-energy band structure and optical excitations. The contributions from the intersite interaction in the other configurations are much smaller in optical response. The result would not change when we slightly overestimate them by V in the facing configuration, because the renormalized part to the transfer integral appears as the product of V and a density matrix [see Eq. (12)] and it was found that the intersite density-matrix elements are almost zero except for that of the facing configuration in the present GaAs case. Therefore, we calculate the V value in the facing configuration and employ it as the V value of the CNDO model.

TABLE I. Interaction parameters determined in the present downfolding procedure. The energy unit is eV.

U_{Ga}	U'_{Ga}	U_{As}	U'_{As}	V
2.39	2.17	2.71	2.09	0.71

The actual determination of the V parameter proceeds as follows: We first choose two decoupled sites (the Ga site placed at the origin and the neighboring As site being in the [111] direction). The similar cutting treatment to Eq. (5) but extending the single-site-cutting formalism to the double-site-cutting formalism is applied for this purpose. Then, we perform constrained calculations by imposing a constraint that two occupancies of the Wannier orbitals $|w_{\mu I\mathbf{0}}\rangle$ and $|w_{\nu J\mathbf{0}}\rangle$ in the facing configuration are kept at $q_{\mu I\mathbf{0}}$ and $q_{\nu J\mathbf{0}}$, respectively. We then draw the two-dimensional potential-energy surface with respect to the constrained parameters $q_{\mu I\mathbf{0}}$ and $q_{\nu J\mathbf{0}}$, and perform a fitting of the quadratic function $\frac{1}{2}U_{\mathrm{Ga}}(q_{\mu I\mathbf{0}}-\bar{q}_{\mu I\mathbf{0}})^2+\frac{1}{2}U_{\mathrm{As}}(q_{\nu J\mathbf{0}}-\bar{q}_{\nu J\mathbf{0}})^2+V(q_{\mu I\mathbf{0}}-\bar{q}_{\mu I\mathbf{0}})(q_{\nu J\mathbf{0}}-\bar{q}_{\nu J\mathbf{0}})$ to the potential-energy data. This fitting is performed by fixing U_{Ga} and U_{As} at predetermined values in the preceding U and U' determination; we treat only V as a single fitting parameter to avoid fitting errors and uncertainties. The V value thus determined is 0.71 eV, where we again see the large reduction from the bare interaction value $V^0=7.35$ eV. The resulting interaction parameters are summarized in Table I.

In general, the downfolded model contains an energy dependence in the interaction because the screening by the high-energy electrons necessarily causes a non-Markoffian and retardation effect. Such an energy dependence in the screened Coulomb interaction $W(\omega)$ is not described by the effective Hamiltonian. However, in the low-energy region, the screened Coulomb interaction is normally saturated to a constant and represented by the limiting value at $\omega=0$. The constrained scheme is roughly regarded as the procedure to obtain this $\omega=0$ limit. The effect of the larger (less screened) interaction W at larger ω as well as the effective interaction arising from virtual transition to eliminated bands can be accounted by the further consideration of the self-energy effect on the low-energy part.[16] For a wide band system such as GaAs, however, this effect may not be large[10] and we thus ignore this effect.

D. Hartree–Fock approximation

In the electronic structure calculation of a typical semiconductor, GaAs, we expect that the strong correlation effect does not appear in the ground state and the HF solution of the CNDO model [Eqs. (1)–(3)] with the effective interactions parametrized in Sec. II C provides us a reasonable re-

sult, although the excitation spectra are reliably determined only through the account of the correlation effect more accurately. In this section, we consider how the HF solution for the ground state is calculated.

The CNDO-HF Hamiltonian in the basis representation of MLWFs is written as

$$\mathcal{H}_{\mathrm{HF}} = \sum_{\sigma} \sum_{\boldsymbol{R}\boldsymbol{R}'} \sum_{ij} \sum_{\mu\nu} F_{\mu i \nu j}(\boldsymbol{R}' - \boldsymbol{R}) a^{\sigma\dagger}_{\mu i \boldsymbol{R}} a^{\sigma}_{\nu j \boldsymbol{R}'}, \tag{11}$$

where $F_{\mu i \nu j}(\boldsymbol{R}' - \boldsymbol{R})$ is the Fock matrix or the renormalized transfer matrix by the interaction part $\mathcal{H}_C$ of Eq. (3) and the matrix element is given by

$$F_{\mu i \nu j}(\boldsymbol{R}' - \boldsymbol{R}) = \begin{cases} I_{\mu i} + \left\{ (Q_i(\boldsymbol{0}) - Z_i) - \frac{1}{2}[Q_{\mu i \mu i}(\boldsymbol{0}) - 2] \right\} U_i + \sum_{\boldsymbol{R}'' k} [Q_k(\boldsymbol{R}'' - \boldsymbol{R}) - Z_k] V_{ik}(\boldsymbol{R}'' - \boldsymbol{R}) & (\boldsymbol{R} = \boldsymbol{R}', i = j, \mu = \nu) \\ t_{\mu i \nu i}(\boldsymbol{0}) - \frac{1}{2} Q_{\mu i \nu i}(\boldsymbol{0}) U'_i & (\boldsymbol{R} = \boldsymbol{R}', i = j, \mu \neq \nu) \\ t_{\mu i \nu j}(\boldsymbol{0}) - \frac{1}{2} Q_{\mu i \nu j}(\boldsymbol{0}) V_{ij}(\boldsymbol{0}) & (\boldsymbol{R} = \boldsymbol{R}', i \neq j) \\ t_{\mu i \nu j}(\boldsymbol{R}' - \boldsymbol{R}) - \frac{1}{2} Q_{\mu i \nu j}(\boldsymbol{R}' - \boldsymbol{R}) V_{ij}(\boldsymbol{R}' - \boldsymbol{R}) & (\boldsymbol{R} \neq \boldsymbol{R}'). \end{cases} \tag{12}$$

Here, $\boldsymbol{Q}(\boldsymbol{R}' - \boldsymbol{R})$ is the density matrix and the matrix element is given by $Q_{\mu i \nu j}(\boldsymbol{R}' - \boldsymbol{R}) = \langle \Phi_{\mathrm{HF}} | \Sigma_{\sigma} a^{\sigma\dagger}_{\mu i \boldsymbol{R}} a^{\sigma}_{\nu j \boldsymbol{R}'} | \Phi_{\mathrm{HF}} \rangle$, where $|\Phi_{\mathrm{HF}}\rangle$ is the HF ground state. The HF Hamiltonian can be diagonalized with the Bloch orbital, $f^{\sigma\dagger}_{\alpha \boldsymbol{k}} = (1/\sqrt{N}) \Sigma_{\mu i} C^{\alpha}_{\mu i}(\boldsymbol{k}) \Sigma_{\boldsymbol{R}} e^{i\boldsymbol{k}\cdot\boldsymbol{R}} a^{\sigma\dagger}_{\mu i \boldsymbol{R}}$, where α and $\boldsymbol{k}$ are a band index and a wave vector, respectively, and N is the total number of the unit cells in the system. The coefficients $\{C^{\alpha}_{\mu i}(\boldsymbol{k})\}$ are determined by solving the following Hartree–Fock equation:

$$\sum_{ij} \sum_{\mu\nu} F_{\mu i \nu j}(\boldsymbol{k}) C^{\alpha}_{\nu j}(\boldsymbol{k}) = \epsilon_{\alpha \boldsymbol{k}} C^{\alpha}_{\mu i}(\boldsymbol{k}) \tag{13}$$

with

$$F_{\mu i \nu j}(\boldsymbol{k}) = \frac{1}{N} \sum_{\boldsymbol{R}} F_{\mu i \nu j}(\boldsymbol{R}) e^{i\boldsymbol{k}\cdot\boldsymbol{R}}. \tag{14}$$

With the resulting $C^{\alpha}_{\mu i}(\boldsymbol{k})$, the real-space density matrix is calculated by

$$Q_{\mu i \nu j}(\boldsymbol{R}) = \frac{1}{N} \sum_{\boldsymbol{k}}^{N} Q_{\mu i \nu j}(\boldsymbol{k}) e^{-i\boldsymbol{k}\cdot\boldsymbol{R}} \tag{15}$$

with

$$Q_{\mu i \nu j}(\boldsymbol{k}) = 2 \sum_{\alpha}^{occ} C^{\alpha}_{\mu i}(\boldsymbol{k}) C^{\alpha *}_{\nu j}(\boldsymbol{k}). \tag{16}$$

The CNDO total energy with the HF approximation is given by

$$E_{\mathrm{tot}} = \langle \Phi_{\mathrm{HF}} | \mathcal{H} | \Phi_{\mathrm{HF}} \rangle = \frac{1}{2} \sum_{\boldsymbol{k}} \sum_{ij} \sum_{\mu\nu} Q_{\mu i \nu j}(\boldsymbol{k}) [H^{\mathrm{core}}_{\nu j \mu i}(\boldsymbol{k}) + F_{\nu j \mu i}(\boldsymbol{k})], \tag{17}$$

where

$$H^{\mathrm{core}}_{\mu i \nu j}(\boldsymbol{k}) = \frac{1}{N} \sum_{\boldsymbol{R}} H^{\mathrm{core}}_{\mu i \nu j}(\boldsymbol{R}) e^{i\boldsymbol{k}\cdot\boldsymbol{R}}. \tag{18}$$

The matrix element of the core matrix $H^{\mathrm{core}}_{\mu i \nu j}(\boldsymbol{R})$ is written as

$$H^{\mathrm{core}}_{\mu i \nu j}(\boldsymbol{R}) = \begin{cases} I_{\mu i} - (Z_i - 1) U_i - \sum_{\boldsymbol{R}' j} Z_j V_{ij}(\boldsymbol{R}') & (\boldsymbol{R} = 0, i = j, \mu = \nu) \\ t_{\mu i \nu j}(\boldsymbol{R}) & (\text{otherwise}). \end{cases} \tag{19}$$

The actual CNDO-HF calculation proceeds along the schematic diagram shown in Fig. 3. The initial density matrix is made from diagonalizing the core matrix $\boldsymbol{H}^{\mathrm{core}}(\boldsymbol{k})$ of Eq. (18). Since the Fock matrix $\boldsymbol{F}(\boldsymbol{R})$ in Eq. (12) depends on the density matrix $\boldsymbol{Q}(\boldsymbol{R})$ of Eq. (15), the HF equation (13) is self-consistently solved with an iterative procedure. To check the convergence, we monitor a density-matrix difference,

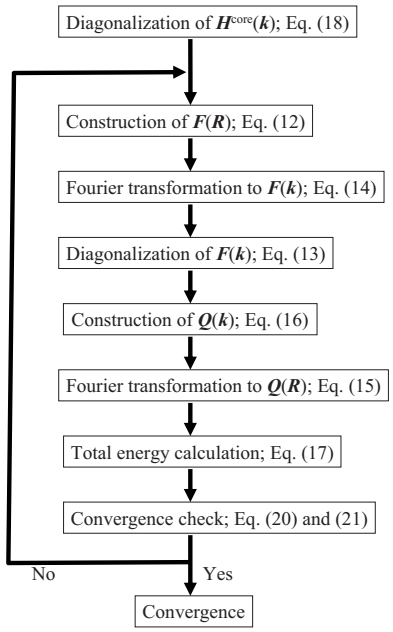

FIG. 3. Schematic diagram for CNDO-HF band calculation.

$$\delta Q^{(i)} = \sqrt{\left(\frac{1}{8}\right)^2 \sum_{ij} \sum_{\mu\nu} [Q^{(i)}_{\mu i \nu j}(\mathbf{0}) - Q^{(i-1)}_{\mu i \nu j}(\mathbf{0})]}, \qquad (20)$$

and a total-energy difference,

$$\delta E^{(i)}_{\mathrm{tot}} = E^{(i)}_{\mathrm{tot}} - E^{(i-1)}_{\mathrm{tot}}, \qquad (21)$$

where an upper suffix i stands for the number of the iteration step. The self-consistency condition we employ is satisfied when $\delta Q^{(i)} \leq 10^{-5}$ a.u. and $\delta E^{(i)}_{\mathrm{tot}} \leq 10^{-6}$ a.u.

We show in Fig. 4 the self-consistent CNDO band structures (solid line), together with the *ab initio* interpolated band (dots). We see a rigid band shift in the conduction band. This rigid band shift is attributed to the renormalization of the interaction part $\mathcal{H}_C$ in Eq. (3) into the one-body part, the so-called self-energy correction considered within the HF framework [see Eq. (12)]. We note that the trend of the rigid band shift is basically the same as the quasiparticle band shift observed in the GW calculation for semiconductor.[12,13]

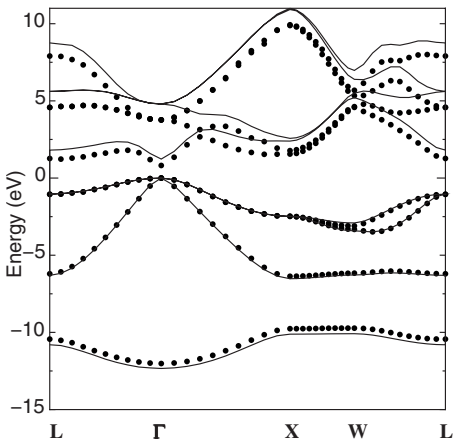

FIG. 4. Self-consistent GaAs CNDO-HF band structure (solid line) and *ab initio* interpolated band structure (dots). Energy zero is set to the top of the valence bands.

III. ELECTRONIC EXCITATION

In Sec. II, we have described the procedure for the downfolding. We now start calculating physical quantities using the downfolded model. The purpose of this section is to examine the reliability of the model obtained by the downfolding. In particular, we highlight whether the model gives us reliable excitation spectra and dynamical properties. For this purpose, we calculate optical absorption spectra, based on a CI treatment considering electron-hole interactions, and compare the computational result to the experiments.

A. Single-excitation configuration interaction

For electrons in solids, the number of configurations generated by the electronic excitations is in principle infinitely large, while the configurations capable of practical computations are limited. Since we are interested in optical processes, we consider here only the SE configurations, which play a primarily important role in the linear absorption process, because the SE configurations directly couple with the HF ground state via an electric dipole operator. The calculation at the SECI level, in fact, takes into account electron-hole interactions; the so-called excitonic effect in the spectrum.

The SECI many-body wave function with a wave vector $\boldsymbol{K}$ is written as[44]

$$|\Psi_{e\boldsymbol{K}}\rangle = \sum_{\boldsymbol{k}} \sum_{a}^{\mathrm{occ}} \sum_{r}^{\mathrm{vir}} \tilde{C}^{e\boldsymbol{K}}_{ark} |{}^1\Psi^{r\boldsymbol{k}+\boldsymbol{K}}_{ak}\rangle, \qquad (22)$$

where $|{}^1\Psi^{r\boldsymbol{k}+\boldsymbol{K}}_{ak}\rangle$ is a spin-singlet SE configuration given by

$$|{}^1\Psi^{r\boldsymbol{k}+\boldsymbol{K}}_{ak}\rangle = \frac{1}{\sqrt{2}}(d^{\uparrow\dagger}_{r\boldsymbol{k}+\boldsymbol{K}} d^{\uparrow}_{ak} + d^{\downarrow\dagger}_{r\boldsymbol{k}+\boldsymbol{K}} d^{\downarrow}_{ak})|\Phi_{\mathrm{HF}}\rangle. \qquad (23)$$

Here, $d^{\sigma\dagger}_{r\boldsymbol{k}}$ (d^{σ}_{ak}) is a creation (annihilation) operator of the Bloch electron in a virtual r (occupied a) band with spin σ and a wave vector $\boldsymbol{k}$. The CI coefficients $\{\tilde{C}^{e\boldsymbol{K}}_{ark}\}$ in Eq. (22) and the excitation energy $\Delta E_{e\boldsymbol{K}}$ are obtained by solving the following CI equation:

$$\sum_{\boldsymbol{k}'} \sum_{b}^{\mathrm{occ}} \sum_{s}^{\mathrm{vir}} A^{\boldsymbol{K}}_{ark,bsk'} \tilde{C}^{e\boldsymbol{K}}_{bsk'} = \Delta E_{e\boldsymbol{K}} \tilde{C}^{e\boldsymbol{K}}_{ark} \qquad (24)$$

with

$$\begin{aligned} A^{\boldsymbol{K}}_{ar\mathbf{k},bsk'} &= \langle {}^1\Psi^{r\boldsymbol{k}+\boldsymbol{K}}_{ak} | \mathcal{H} - E_{\mathrm{HF}} | {}^1\Psi^{s\boldsymbol{k}'+\boldsymbol{K}}_{bk'} \rangle \\ &= (\epsilon_{r\boldsymbol{k}+\boldsymbol{K}} - \epsilon_{ak}) \delta_{\boldsymbol{k}\boldsymbol{k}'} \delta_{ab} \delta_{rs} + 2\langle r_{\boldsymbol{k}+\boldsymbol{K}} a_{\boldsymbol{k}} | b_{\boldsymbol{k}'} s_{\boldsymbol{k}'+\boldsymbol{K}} \rangle \\ &\quad - \langle r_{\boldsymbol{k}+\boldsymbol{K}} s_{\boldsymbol{k}'+\boldsymbol{K}} | b_{\boldsymbol{k}'} a_{\boldsymbol{k}} \rangle, \end{aligned} \qquad (25)$$

where E_{HF} is the HF ground-state eigenenergy for the many-body HF Hamiltonian $\mathcal{H}_{\mathrm{HF}}$ in Eq. (11); $\mathcal{H}_{\mathrm{HF}}|\Phi_{\mathrm{HF}}\rangle = E_{\mathrm{HF}}|\Phi_{\mathrm{HF}}\rangle$. For the CNDO model, the second term in Eq. (25), called the exchange term, is calculated as

$$\langle r_{\boldsymbol{k}+\boldsymbol{K}} a_{\boldsymbol{k}} | b_{\boldsymbol{k}'} s_{\boldsymbol{k}'+\boldsymbol{K}} \rangle = \sum_{\mu i} \sum_{\nu j} C^{r*}_{\mu i}(\boldsymbol{k}+\boldsymbol{K}) C^{a}_{\mu i}(\boldsymbol{k}) \times C^{b*}_{\nu j}(\boldsymbol{k}') C^{s}_{\nu j}(\boldsymbol{k}'+\boldsymbol{K}) \mathcal{V}_{\mu i \nu j}(\boldsymbol{K}), \quad (26)$$

and the last term in Eq. (25), referred to as the direct term, is evaluated by

$$\langle r_{\boldsymbol{k}+\boldsymbol{K}} s_{\boldsymbol{k}'+\boldsymbol{K}} | b_{\boldsymbol{k}'} a_{\boldsymbol{k}} \rangle = \sum_{\mu i} \sum_{\nu j} C^{r*}_{\mu i}(\boldsymbol{k}+\boldsymbol{K}) C^{s}_{\mu i}(\boldsymbol{k}'+\boldsymbol{K}) C^{b*}_{\nu j}(\boldsymbol{k}') \times C^{a}_{\nu j}(\boldsymbol{k}) \mathcal{V}_{\mu i \nu j}(\boldsymbol{k}-\boldsymbol{k}'), \quad (27)$$

with

$$\mathcal{V}_{\mu i \nu j}(\boldsymbol{k}) = \frac{1}{N} \sum_{\boldsymbol{R}} \mathcal{V}_{\mu i \nu j}(\boldsymbol{R}) e^{i\boldsymbol{k}\cdot\boldsymbol{R}} \quad (28)$$

and

$$\mathcal{V}_{\mu i \nu j}(\boldsymbol{R}) = \begin{cases} U_i & (\boldsymbol{R}=\boldsymbol{0}, i=j, \mu=\nu) \\ U'_i & (\boldsymbol{R}=\boldsymbol{0}, i=j, \mu\neq\nu) \\ V_{ij}(\boldsymbol{R}) & (\text{otherwise}). \end{cases} \quad (29)$$

Equations (26) and (27) imply the repulsive-exchange and attractive-Coulomb interactions between an electron in the r and s bands and a positive hole in the a and b bands, with the total wave vector being kept constant $[(\boldsymbol{k}+\boldsymbol{K})-\boldsymbol{k}=\boldsymbol{K}]$.

The structure of the present CNDO-HF-SECI Eq. (24) is basically the same as that of the Bethe–Salpeter equation for two-particle Green's functions.[8,10,11] A difference is that the former electron-electron interaction in the two-electron integrals of Eqs. (26) and (27) is represented by $\mathcal{V}_{\mu i \nu j}(\boldsymbol{R})$ determined via the constrained scheme (see Sec. II C), while the latter interaction is represented by the screened Coulomb interaction evaluated with the random phase approximation. Computationally, we note that four-center Coulomb integrals in the original exchange and/or direct terms are reduced to two-center Coulomb integrals including only the sites i and j because of the CNDO approximation.[36] Therefore, the computational cost for the matrix evaluation is much smaller in our CI calculation. The most time consuming step is the diagonalization of the CI matrix $\boldsymbol{A}^{\boldsymbol{K}}$, which is scaled as the third power of the dimension of the $\boldsymbol{A}^{\boldsymbol{K}}$; $(N \times N_{\mathrm{occ}} \times N_{\mathrm{vir}})^3$.

B. Optical absorption

We next describe the expression for the SECI optical absorption, which is given as the imaginary part of the macroscopic transverse dielectric function,[5]

$$\epsilon_2(\omega) = \mathcal{N} \sum_{e} |\langle \Psi_{e\boldsymbol{K}=\boldsymbol{0}} | \boldsymbol{X} | \Phi_{\mathrm{HF}} \rangle|^2 \delta(\Delta E_{e\boldsymbol{K}=\boldsymbol{0}} - \omega), \quad (30)$$

where $\boldsymbol{X}=\Sigma_i \boldsymbol{r}_i$ is a many-body position operator of electrons, and the normalization constant $\mathcal{N}$ is determined via the following sum rule:[45]

$$\int_0^\infty \omega \epsilon_2(\omega) d\omega = \frac{\pi}{2} \omega_p^2 \quad (31)$$

with ω_p being the plasma frequency of the system. Substituting Eq. (22) into Eq. (30) and noting the commutation relation $[\mathcal{H}_{\mathrm{HF}}, \boldsymbol{X}] = \Sigma_i [\hat{h}_{\mathrm{HF}}(i), \boldsymbol{r}_i] = -\Sigma_i \partial / \partial \boldsymbol{r}_i$, we obtain

$$\epsilon_2(\omega) = \mathcal{N} \sum_{e} \left| \sum_{\boldsymbol{k}} \sum_{a}^{occ} \sum_{r}^{\mathrm{vir}} \tilde{C}^{e\boldsymbol{K}=\boldsymbol{0}}_{ar\boldsymbol{k}} \frac{\langle \phi_{r\mathbf{k}} | \partial / \partial \boldsymbol{r} | \phi_{a\boldsymbol{k}} \rangle}{\epsilon_{r\boldsymbol{k}} - \epsilon_{a\boldsymbol{k}}} \right|^2 \times \delta(\Delta E_{e\boldsymbol{K}=\boldsymbol{0}} - \omega), \quad (32)$$

where $|\phi_{a\boldsymbol{k}}\rangle$ is the Bloch state being the eigenstate of the Fock operator $\hat{h}_{\mathrm{HF}}$ and the matrix element of $\partial / \partial \boldsymbol{r}$ can be calculated with an interpolation scheme[46] based on the ML-WFs from first principles (see Appendix B). Theoretically, $\epsilon_2(\omega)$ contains an electron-hole-interaction effect due to the presence of the CI coefficients in Eq. (32). To see the electron-hole-interaction effect on the spectrum, it is convenient to compare it to the spectrum obtained by the independent-particle approximation[47] (IPA) where the CI coefficients are neglected in Eq. (32) and the excitations are described just with optical transitions between independent hole and electron states,

$$\epsilon_2^{(0)}(\omega) = \mathcal{N} \sum_{\boldsymbol{k}} \sum_{a}^{occ} \sum_{r}^{\mathrm{vir}} \left| \frac{\langle \phi_{r\boldsymbol{k}} | \partial / \partial \boldsymbol{r} | \phi_{a\boldsymbol{k}} \rangle}{\epsilon_{r\boldsymbol{k}} - \epsilon_{a\boldsymbol{k}}} \right|^2 \delta(\epsilon_{r\boldsymbol{k}} - \epsilon_{a\boldsymbol{k}} - \omega). \quad (33)$$

In the spectral calculations, we have chosen a k grid different from the Monkhorst–Pack k grid used in the band calculations.[10] The present k grid is generated as follows: We first make a uniform k grid in an $11 \times 11 \times 11$ Monkhorst–Pack mesh and then slightly shift uniformly the sampling $\boldsymbol{k}$ in the direction of $-0.01\boldsymbol{b}_1 - 0.02\boldsymbol{b}_2 + 0.03\boldsymbol{b}_3$ with $\{\boldsymbol{b}_1, \boldsymbol{b}_2, \boldsymbol{b}_3\}$ being basic reciprocal-lattice vectors. The resulting k points are different from the high-symmetry directions of the crystal and therefore are not connected via rotational operations of the crystal with each other. This leads to a finer sampling for the spectral calculation. An unshifted grid corresponds to only 56 crystallographically different points, which are too few to achieve a good spectral resolution. On the other hand, the shifted grid leads to a grid of 1331 crystallographically different k points, which gives a good spectral resolution.

We show in Fig. 5 the calculated SECI (thick red line) and IPA (thin green line) spectra. The closed blue and open blue circles denote experimental results.[30,31] We see a clear con-

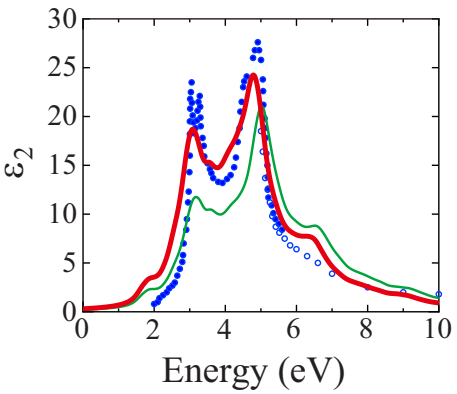

FIG. 5. (Color online) Calculated SECI (thick red line) and IPA (thin green line) optical absorption spectrum of GaAs. The closed blue and open blue circles represent experimental data taken from Refs. 30 and 31, respectively.

trast between the SECI and IPA spectra; by considering the electron-hole interaction with the SECI method, the spectral intensity in the low-energy region (≤ 5 eV) is enhanced, thus perfectly reproducing the experimental results. The agreement is indeed somewhat surprising, when we consider the several simplified treatments employed here such as the reduction of the electron-electron interaction to the extended Hubbard form. However, we emphasize that the nature such as the spectral enhancement observed in proceeding from IPA to SECI is consistent with highly accurate full *ab initio* results[10,11] obtained from solving the Bethe–Salpeter equations. In the context of the downfolding, these results strongly support that our model construction by the downfolding described in Sec. II C offers a reliable description not only of the ground-state band structure but also of the excitation spectra.

For completeness, we perform a more critical and elaborate assessment of the reliability of the downfolding; we examine a sensitivity of the spectra to choices of Hamiltonian parameters. In the present analysis, we focus on the check of the reliability of the off-site interaction parameter V. In fact, the magnitude of this parameter is expected to crucially control the strength of the electron-hole interaction [see Eqs. (26) and (27)] and thus directly affect the profile of the optical spectra. We may calculate the excitation spectra by using choices of interaction parameters different from the downfolded realistic values. Thus, the reliability of the downfolding can be assessed by examining whether the spectrum obtained from the present downfolded Hamiltonian gives the best agreement with the experiment among wider alternative choices of the interaction parameters. For this check, we introduce a scaling factor x to scale V to xV. With this definition, $x=1$ corresponds to the original *ab initio* V value, while in the region $x>1$, the nearest-neighbor electron-electron repulsion is artificially overestimated. In the practical calculation, we monitor the values of x at 0.8, 1.0, and 1.2 and then perform the SECI calculations to obtain the optical spectra for each V value. (In the calculations, the on-site parameters are fixed at the *ab initio* determined values displayed in Table I.)

We show in Fig. 6 the resulting dependence of the SECI spectra (red lines) on the scaling factor x. The blue circles denote measured data. We see a notable change in the spectra due to the parameter increase [(a)→(b)→(c)]; increasing x makes a blueshift and an intensity decrease in the calculated spectra. We see that the spectrum at the downfolded choice (i.e., the case with $x=1.0$) exhibits the best agreement with the experiments among all the choices. The downfolded value offers the most realistic and accurate choices as the model parameters, and thus we conclude that the optical excitation spectrum is correctly captured by the downfolded Hamiltonian.

Finally, we remark a recent development for *ab initio* evaluations for the off-site V parameter. Indeed, applications of the constrained schemes to the determinations of the off-site parameter is quite limited in the literature compared to those for the on-site parameters. Recently, Aryasetiawan *et al.*[16] have proposed an RPA approach for calculating the interaction parameters. They first calculated a real-space screened Coulomb interaction $U(\boldsymbol{r},\boldsymbol{r}')$ by excluding the polarization formed in target bands contained in the model Hamiltonian and then evaluated the matrix element of U in the localized basis such as linearized muffin-tin orbitals and/or maximally localized Wannier functions. This approach is able to derive all of the off-site parameters included in the effective interaction having a long-range tail. This point becomes essential when we consider a problem concerning strong bound excitons formed in ionic crystal such as LiF,[10] which reflects the long-range Coulomb interaction due to a poor screening associated with a low dielectric constant. For the description of spectral behavior of such systems, we need to take into account the long-range behavior in the effective interaction. For this purpose, the constrained RPA technique is more suitable than the presented constrained LDA approach, because, in the RPA calculation, all of the parameters can be evaluated in a primitive-cell calculation and there is no difficulty arising from the size of the supercell, which exists in the constrained LDA calculations. For example, in the constrained LDA, as the length scale of the interaction increases, a larger size of the supercell is required. The relation between the constrained RPA and the constrained LDA is somewhat complicated because of the different derivations in the two methods,[16–18] so their com-

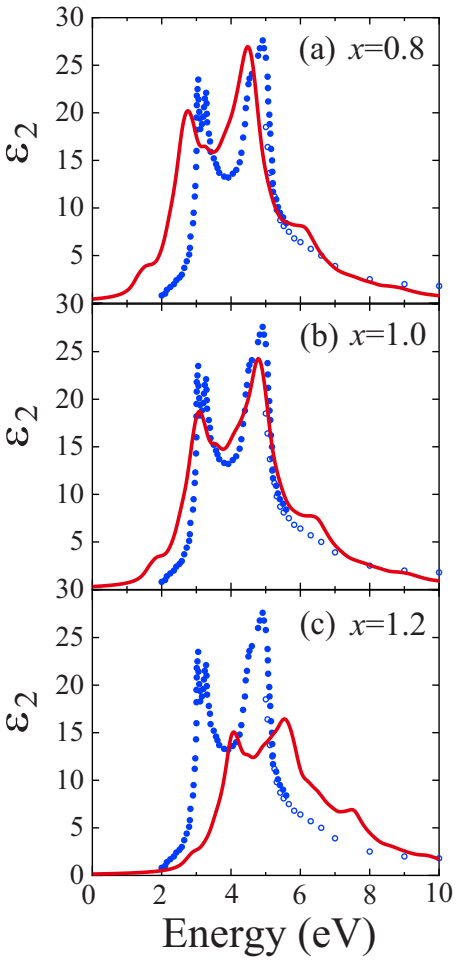

FIG. 6. (Color online) Dependence of SECI spectra (red lines) on scaling factor x; (a) $x=0.8$, (b) $x=1.0$, and (c) $x=1.2$. The closed blue and open blue circles represent experimental data taken from Refs. 30 and 31, respectively.

parisons for the numerical aspect are highly desirable for elucidating the range of applicability of these techniques in deriving the interaction parameters, which will be discussed elsewhere.

IV. CONCLUSIONS

We have examined whether the effective low-energy Hamiltonian derived from the downfolding procedure is able to describe dynamics and excitation spectra in a proper way. The calculation is performed in the three-stage scheme. In the first stage, we calculate the global electronic structure from the density-functional theory supplemented by the generalized gradient approximation. The high-energy degrees of freedom in the global electronic band structure are, in the second stage, eliminated by the downfolding scheme, which leaves only the low-energy bands near the Fermi level. In the present example of GaAs, we retain up to 25 Ry for the calculation of the global electronic bands, while the downfolded Hamiltonian keeps only eight bands near the Fermi level up to 15 eV ($\sim$1 Ry). By the downfolding, kinetic and interaction energies are separately renormalized into the low-energy eight bands and the effective Hamiltonian, where we employ the CNDO model neglecting the off-diagonal part of the Coulomb interaction, is constructed from first principles, with the help of the maximally localized Wannier functions. This procedure, although several simplified treatments are employed, in principle, does not contain any *ad hoc* parameters. In the third stage, the Hartree–Fock method for the ground state supplemented by the single-excitation configuration-interaction treatment for considering the electron-hole interactions has been applied to obtain electronic excitation spectra of semiconductor GaAs. The spectra thus obtained have quite well reproduced the experimental results; the intensity and position for the excitonic peak are well reproduced at a quantitative level. We believe that the present model construction based on the downfolding offers a reliable *ab initio* scheme, where the downfolded effective Hamiltonian is capable of not only the ground-state properties but also the excitation spectra.

The present result opens a way of treating excitations such as the optical spectra by the hybrid method combining the density-functional approach and the accurate low-energy solver for the low-energy effective models. Beyond the present application to semiconductors, it would be interesting to apply this approach to excitations in strongly correlated electron systems such as transition-metal oxides including the cuprates. In the present paper, we have used the Hartree–Fock approximation for the ground state and the single-excitation configuration-interaction treatment for the excitations. Optical excitation spectra of GaAs have satisfactorily been treated by these approximations and the experimental results have been well reproduced. However, stronger electron correlation effects require a more sophisticated low-energy solver than the Hartree–Fock/single-excitation configuration-interaction treatment. For more different and challenging issues of the electron correlation, the low-energy effective Hamiltonian may indeed be treated by a much more reliable low-energy solver for electrons in solids, such as quantum Monte Carlo methods for lattice Fermions,[25] path-integral renormalization group method,[24] and cluster extensions of the dynamical mean field theory.[15]

As is well known, there are many direct *ab initio* schemes aiming at considering correlation effects; for example, the GW,[12,13,48] transcorrelated,[21] and quantum Monte Carlo methods.[20] They are straightforward ways for approaching the problem compared to the present approach. However, the straightforward methods are faced with two serious problems: One is that the computational load becomes extremely heavy when all of the electrons or even all of the valence electrons are equally treated. The other problem is that the so far developed straightforward methods do not offer a sufficiently accurate framework if the electron correlation becomes strong such as in the genuine Mott insulator. The crucial point is that we need to treat dynamical as well as short-range spatial correlations and fluctuations beyond RPA near the Fermi level in a controllable way. In the present stage of the computer power, such sufficient accuracies are undertaken only within simple models, which can be achieved in the low-energy effective model after downfolding. In fact, the high accuracy required from the temporal and spatial quantum fluctuations is important only in the low-energy region near the Fermi level, which justifies to restrict the high-accuracy treatment only in the region of low-energy excitations and thus only within the downfolded Hamiltonian. This downfolding procedure opens an avenue of studying highly correlated electron systems as well as excitations without relying on *ad hoc* parameters, if it is combined with an appropriate and accurate low-energy solver recently developed for low-energy Hamiltonians. Explicit consideration of the energy hierarchy in the electronic structure makes the first-principles calculations more tractable even when the electron correlation is essential. An important task left for future progress is to further develop accurate low-energy solvers focused for dynamical and excitation properties.

ACKNOWLEDGMENTS

We would like to thank Takashi Miyake, Atsushi Yamasaki, Youhei Yamaji, Takahiro Misawa, and Taichi Kosugi for helpful discussions and comments. This work was supported by a Grant-in-Aid for Scientific Research in Priority Areas, "Development of New Quantum Simulators and Quantum Design" (Grant No. 17064004) of the Ministry of Education, Culture, Sports, Science and Technology, Japan. One of us (K.N.) acknowledges financial support from the Japan Society for the Promotion of Science for Young Scientists. All of the calculations were performed on Hitachi SR11000 system of the Super Computer Center at the Institute for Solid State Physics, the University of Tokyo.

APPENDIX A: DERIVATION OF THE FITTING FUNCTION OF EQUATION (10)

Here, we describe the details of the fitting function used in the on-site parameter determination. In the atomic limit, the on-site Hamiltonian for the decoupled site I in the home cell is written as

$$\mathcal{H}_C^{I\mathbf{0}} = U_I \sum_{\mu} N_{\mu I\mathbf{0}}^{\uparrow} N_{\mu I\mathbf{0}}^{\downarrow} + U_I' \sum_{\mu<\nu} N_{\mu I\mathbf{0}} N_{\nu I\mathbf{0}} + \epsilon_I \sum_{\mu} N_{\mu I\mathbf{0}}$$
$$= \frac{U_I}{2} \sum_{\mu} N_{\mu I\mathbf{0}}(N_{\mu I\mathbf{0}} - 1) + \frac{U_I'}{2} \sum_{\mu\neq\nu} N_{\mu I\mathbf{0}} N_{\nu I\mathbf{0}} + \epsilon_I \sum_{\mu} N_{\mu I\mathbf{0}}, \tag{A1}$$

where $N_{\mu I\mathbf{0}}^{\sigma}$ and $N_{\mu I\mathbf{0}}=\Sigma_{\sigma} N_{\mu I\mathbf{0}}^{\sigma}$ are number operators. U_I and U_I' are the on-site intraorbital and interorbital Coulomb repulsions, respectively. ϵ_I is a chemical potential. The on-site energy $E_C^{I\mathbf{0}}$ derived from Eq. (A1) is expressed with the atomic-limit wave function $|\Phi_{\mathrm{AL}}\rangle$ as

$$E_C^{I\mathbf{0}} = \langle \Phi_{\mathrm{AL}} | \mathcal{H}_C^{I\mathbf{0}} | \Phi_{\mathrm{AL}} \rangle$$
$$= \frac{U_I}{2} \sum_{\mu} q_{\mu I\mathbf{0}}(q_{\mu I\mathbf{0}} - 1) + \frac{U_I'}{2} \sum_{\mu\neq\nu} q_{\mu I\mathbf{0}} q_{\nu I\mathbf{0}} + \epsilon_I \sum_{\mu} q_{\mu I\mathbf{0}}, \tag{A2}$$

where we used $N_{\mu I\mathbf{0}}|\Phi_{\mathrm{AL}}\rangle = q_{\mu I\mathbf{0}}|\Phi_{\mathrm{AL}}\rangle$. We introduce $\delta q_{\mu I\mathbf{0}} = q_{\mu I\mathbf{0}} - \bar{q}_{I\mathbf{0}}$ with $\bar{q}_{I\mathbf{0}}$ defined as the orbital occupancy at the equilibrium state. At the equilibrium state, the term linear in $\delta q_{\mu I\mathbf{0}}$ should vanish, which results in cancellation of the chemical potential term with the linear term from the Coulomb contribution. Then, the quadratic energy difference due to the charge fluctuations is derived as

$$\Delta E_C^{I\mathbf{0}} = \frac{U_I}{2} \sum_{\mu} (\delta q_{\mu I\mathbf{0}})^2 + \frac{U_I'}{2} \sum_{\mu\neq\nu} \delta q_{\mu I\mathbf{0}} \delta q_{\nu I\mathbf{0}}. \tag{A3}$$

By noting $\Sigma_{\mu}(\delta q_{\mu I\mathbf{0}})^2 = (\Sigma_{\mu} \delta q_{\mu I\mathbf{0}})^2 - \Sigma_{\mu\neq\nu} \delta q_{\mu I\mathbf{0}} \delta q_{\nu I\mathbf{0}}$ and defining the site-charge fluctuation $\delta Q_{I\mathbf{0}} = (\Sigma_{\mu} \delta q_{\mu I\mathbf{0}})$, we obtain the following form:

$$\Delta E_C^{I\mathbf{0}} = \frac{U_I}{2} (\delta Q_{I\mathbf{0}})^2 + \frac{1}{2}(U_I' - U_I) \sum_{\mu\neq\nu} \delta q_{\mu I\mathbf{0}} \delta q_{\nu I\mathbf{0}}. \tag{A4}$$

One may specialize the charge fluctuation of one orbital because of the crystallographical symmetry in the system. Thus, the orbital index in the orbital-charge fluctuation is dropped and the cross term in Eq. (A4) is rewritten in terms of $\delta Q_{I\mathbf{0}}$ and $\delta q_{I\mathbf{0}}$,

$$\sum_{\mu\neq\nu} \delta q_{\mu I\mathbf{0}} \delta q_{\nu I\mathbf{0}} = 4 \delta q_{I\mathbf{0}} (\delta Q_{I\mathbf{0}} - \delta q_{I\mathbf{0}}). \tag{A5}$$

Inserting the above expression into Eq. (A4) leads to the following expression for the on-site interaction energy:

$$\Delta E_C^{I\mathbf{0}} = \frac{U_I}{2} (\delta Q_{I\mathbf{0}})^2 + 2(U_I' - U_I) \delta Q_{I\mathbf{0}} \delta q_{I\mathbf{0}}$$
$$+ [2(U_I - U_I')](\delta q_{I\mathbf{0}})^2. \tag{A6}$$

APPENDIX B: EVALUATION OF THE MATRIX ELEMENT OF $\partial/\partial \boldsymbol{r}$

Here, we describe details for the calculation of the matrix element $\langle \phi_{r\boldsymbol{k}} | \partial/\partial \boldsymbol{r} | \phi_{a\boldsymbol{k}} \rangle$ in Eq. (32). We first rewrite it in terms of the maximally localized Wannier function as

$$\langle \phi_{r\boldsymbol{k}} | \frac{\partial}{\partial \boldsymbol{r}} | \phi_{a\boldsymbol{k}} \rangle = \frac{1}{N} \sum_{\mu\nu} \sum_{ij} \sum_{\boldsymbol{R}\boldsymbol{R}'} C_{\mu i}^{r*}(\boldsymbol{k}) C_{\nu j}^{a}(\boldsymbol{k})$$
$$\times e^{i\mathbf{k}\cdot(\boldsymbol{R}'-\boldsymbol{R})} \langle w_{\mu i\boldsymbol{R}} | \frac{\partial}{\partial \boldsymbol{r}} | w_{\nu j\boldsymbol{R}'} \rangle \tag{B1}$$

with $|\phi_{a\boldsymbol{k}}\rangle = (1/\sqrt{N}) \Sigma_{\mu i} C_{\mu i}^{\alpha}(\boldsymbol{k}) \Sigma_{\boldsymbol{R}} e^{i\boldsymbol{k}\cdot\boldsymbol{R}} |w_{\mu i\boldsymbol{R}}\rangle$. In our calculation, the Wannier function $w_{\mu i}(\boldsymbol{r}-\boldsymbol{R}) = \langle \boldsymbol{r} | w_{\mu i\boldsymbol{R}} \rangle$ is stored as numerical data on the real-space grid,

$$\boldsymbol{r} = \frac{m_1}{M_1} \boldsymbol{L}_1 + \frac{m_2}{M_2} \boldsymbol{L}_2 + \frac{m_3}{M_3} \boldsymbol{L}_3, \tag{B2}$$

where $\boldsymbol{L}_i (= N_i \boldsymbol{a}_i)$ is a cell vector defining a superlattice containing $N (= N_1 N_2 N_3)$ primitive cells, and m_i runs on the integer values: $0, 1, \ldots, M_i - 1$ with M_i being the total number of the grids in the ith direction (in the present case, $M_1 = M_2 = M_3 = 240$). Since the Wannier function satisfies the following periodic boundary condition:

$$w_{\mu i}(\boldsymbol{r} + \boldsymbol{L}_i) = w_{\mu i}(\boldsymbol{r}), \quad i = 1,2,3, \tag{B3}$$

we can express $w_{\mu i}(\boldsymbol{r})$ in terms of the Fourier transformation as

$$w_{\mu i}(\boldsymbol{r}) = \sum_{\mathbf{G}_L} w_{\mu i}(\boldsymbol{G}_L) e^{i\boldsymbol{G}_L \cdot \boldsymbol{r}}, \tag{B4}$$

where $\boldsymbol{G}_L = g_1 \boldsymbol{L}_1^* + g_2 \boldsymbol{L}_2^* + g_3 \boldsymbol{L}_3^*$ with $\boldsymbol{L}_i^* = (2\pi/V) \boldsymbol{L}_j \times \boldsymbol{L}_k$, $V = (\boldsymbol{L}_1 \cdot \boldsymbol{L}_2 \times \boldsymbol{L}_3)$ is the volume of the superlattice, and g_i takes value from 1 to $M_i - 1$. We note that $\boldsymbol{G}_L$ is different from $\boldsymbol{G}$ used in the *ab initio* band calculations; the former is expressed in terms of the reciprocal-lattice vectors for the superlattice $\{\boldsymbol{L}_1^*, \boldsymbol{L}_2^*, \boldsymbol{L}_2^*\}$, while the latter is written with the basic reciprocal-lattice vectors $\{\boldsymbol{b}_1, \boldsymbol{b}_2, \boldsymbol{b}_3\}$. Substituting Eq. (B4) into Eq. (B1) and using the translational symmetry for the matrix element lead to

$$\langle \phi_{r\boldsymbol{k}} | \frac{\partial}{\partial \boldsymbol{r}} | \phi_{a\boldsymbol{k}} \rangle = \sum_{\mu\nu} \sum_{ij} C_{\mu i}^{r*}(\boldsymbol{k}) C_{\nu j}^{a}(\boldsymbol{k}) \sum_{\boldsymbol{R}} g_{\mu i \nu j}(\boldsymbol{R}) e^{i\mathbf{k}\cdot\boldsymbol{R}} \tag{B5}$$

with

$$g_{\mu i \nu j}(\boldsymbol{R}) = iV \sum_{\mathbf{G}_L} w_{\mu i}^*(\boldsymbol{G}_L) w_{\nu j}(\boldsymbol{G}_L) \boldsymbol{G}_L e^{-i\boldsymbol{G}_L \cdot \boldsymbol{R}}. \tag{B6}$$

The actual calculation proceeds as follows: We first transform the real-space Wannier function $w_{\mu i}(\boldsymbol{r})$ into the reciprocal-space one $w_{\mu i}(\boldsymbol{G}_L)$ in Eq. (B4) with the algorithm of the fast Fourier transformation with radix-2, 3, and 5. Then, we calculate the $\partial/\partial \boldsymbol{r}$ matrix in the Wannier basis [$\boldsymbol{g}(\boldsymbol{R})$ in Eq. (B6)] to obtain the desired quantity [Eq. (B5)]. We note that this numerical procedure is a so-called Wannier interpolation scheme;[46] we construct the Wannier functions with the *ab initio* Bloch functions in the Monkhorst–Pack k grid and then interpolate the matrix elements of $\partial/\partial \boldsymbol{r}$ at the slightly shifted k grid used in the spectral calculation.

*kazuma@solis.t.u-tokyo.ac.jp

[1] P. Hohenberg and W. Kohn, Phys. Rev. **136**, B864 (1964).
[2] N. F. Mott, Proc. Phys. Soc., London, Sect. A **62**, 416 (1949); M. C. Gutzwiller, Phys. Rev. Lett. **10**, 159 (1963); J. Hubbard, Proc. R. Soc. London, Ser. A **276**, 238 (1963); J. Kanamori, Prog. Theor. Phys. **30**, 275 (1963).
[3] L. F. Mattheiss, Phys. Rev. B **5**, 290 (1972); L. F. Mattheiss, *ibid.* **5**, 306 (1972); K. Terakura, T. Oguchi, A. R. Williams, and J. Kubler, *ibid.* **30**, 4734 (1984); G. A. Sawatzky and J. W. Allen, Phys. Rev. Lett. **53**, 2339 (1984).
[4] W. Hanke and L. J. Sham, Phys. Rev. Lett. **43**, 387 (1979); Phys. Rev. B **21**, 4656 (1980).
[5] See for example, Y. Toyozawa, *Optical Processes in Solids* (Cambridge University Press, Cambridge, 2003).
[6] W. Kohn and L. J. Sham, Phys. Rev. **140**, A1133 (1965).
[7] C. C. J. Roothaan, Rev. Mod. Phys. **23**, 69 (1951).
[8] S. Albrecht, L. Reining, R. DelSole, and G. Onida, Phys. Rev. Lett. **80**, 4510 (1998); E. L Shirley, *ibid.* **80**, 794 (1998); L. X. Benedict, E. L Shirley, and R. B. Bohn, *ibid.* **80**, 4514 (1998); L. X. Benedict and E. L. Shirley, Phys. Rev. B **59**, 5441 (1999); M. Rohlfing and S. G. Louie, Phys. Rev. Lett. **82**, 1959 (1999); J.-W. van der Horst, P. A. Bobbert, M. A. J. Michels, G. Brocks, and P. J. Kelly, *ibid.* **83**, 4413 (1999); J.-W. van der Horst, P. A. Bobbert, P. H. L. de Jong, M. A. J. Michels, G. Brocks, and P. J. Kelly, Phys. Rev. B **61**, 15817 (2000); P. Puschnig and C. Ambrosch-Draxl, Phys. Rev. B **66**, 165105 (2002); B. Arnaud, S. Lebegue, P. Rabiller, and M. Alouani, Phys. Rev. Lett. **96**, 026402 (2006); For a review, see G. Onida, L. Reining, and A. Rubio, Rev. Mod. Phys. **74**, 601 (2002).
[9] For a time-dependent density-functional approach to the optical problem, see F. Sottile, K. Karlsson, L. Reining, and F. Aryasetiawan, Phys. Rev. B **68**, 205112 (2003); A. Marini, R. DelSole, and A. Rubio, Phys. Rev. Lett. **91**, 256402 (2003).
[10] M. Rohlfing and S. G. Louie, Phys. Rev. Lett. **81**, 2312 (1998); Phys. Rev. B **62**, 4927 (2000).
[11] L. X. Benedict, E. L. Shirley, and R. B. Bohn, Phys. Rev. B **57**, R9385 (1998); B. Arnaud and M. Alouani, *ibid.* **63**, 085208 (2001); P. H. Hahn, K. Seino, W. G. Schmidt, J. Furthmuller, and F. Bechstedt, Phys. Status Solidi B **242**, 2720 (2005).
[12] L. Hedin and S. Lundqvist, *Solid State Physics* (Academic Press, New York, 1969), Vol. 23, p. 1; M. S. Hybertsen and S. G. Louie, Phys. Rev. B **34**, 5390 (1986); M. S. Hybertsen and S. G. Louie, *ibid.* **35**, 5585 (1987); R. W. Godby, M. Schluter, and L. J. Sham, *ibid.* **35**, 4170 (1987); F. Aryasetiawan, *ibid.* **46**, 13051 (1992); F. Aryasetiawan and O. Gunnarsson, Phys. Rev. Lett. **74**, 3221 (1995); F. Aryasetiawan, Rep. Prog. Phys. **61**, 237 (1998).
[13] R. W. Godby, M. Schluter, and L. J. Sham, Phys. Rev. B **37**, 10159 (1988); F. Gygi and A. Baldereschi, Phys. Rev. Lett. **62**, 2160 (1989).
[14] V. I. Anisimov, J. Zaanen, and O. K. Andersen, Phys. Rev. B **44**, 943 (1991); V. I. Anisimov, F. Aryasetiawan, and A. I. Lichtenstein, J. Phys. Condens. Matter **9**, 767 (1997); A. I. Lichtenstein and M. I. Katsnelson, Phys. Rev. B **57**, 6884 (1998).
[15] V. I. Anisimov, A. I. Poteryaev, M. A. Korotin, A. O. Anokhin, and G. Kotliar, J. Phys.: Condens. Matter **9**, 7359 (1997); G. Kotliar, S. Y. Savrasov, K. Haule, V. S. Oudovenko, O. Parcollet, and C. A. Marianetti, Rev. Mod. Phys. **78**, 865 (2006).
[16] F. Aryasetiawan, M. Imada, A. Georges, G. Kotliar, S. Biermann, and A. I. Lichtenstein, Phys. Rev. B **70**, 195104 (2004); F. Aryasetiawan, K. Karlsson, O. Jepsen, and U. Schonberger, *ibid.* **74**, 125106 (2006).
[17] I. V. Solovyev and M. Imada, Phys. Rev. B **71**, 045103 (2005).
[18] I. V. Solovyev, Phys. Rev. B **73**, 155117 (2006).
[19] Y. Imai, I. V. Solovyev, and M. Imada, Phys. Rev. Lett. **95**, 176405 (2005); Y. Imai and M. Imada, J. Phys. Soc. Jpn. **75**, 094713 (2006); Y. Otsuka and M. Imada, *ibid.* **75**, 124707 (2006).
[20] W. M. C. Foulkes, L. Mitas, R. J. Needs, and G. Rajagopal, Rev. Mod. Phys. **73**, 33 (2001).
[21] R. Sakuma and S. Tsuneyuki, J. Phys. Soc. Jpn. **75**, 103705 (2006).
[22] N. Marzari and D. Vanderbilt, Phys. Rev. B **56**, 12847 (1997); I. Souza, N. Marzari, and D. Vanderbilt, *ibid.* **65**, 035109 (2001).
[23] E. Pavarini, S. Biermann, A. Poteryaev, A. I. Lichtenstein, A. Georges, and O. K. Andersen, Phys. Rev. Lett. **92**, 176403 (2004); V. I. Anisimov, D. E. Kondakov, A. V. Kozhevnikov, I. A. Nekrasov, Z. V. Pchelkina, J. W. Allen, S.-K. Mo, H.-D. Kim, P. Metcalf, S. Suga, A. Sekiyama, G. Keller, I. Leonov, X. Ren, and D. Vollhardt, Phys. Rev. B **71**, 125119 (2005); V. I. Anisimov and A. V. Kozhevnikov, *ibid.* **72**, 075125 (2005); F. Lechermann, A. Georges, A. Poteryaev, S. Biermann, M. Posternak, A. Yamasaki, and O. K. Andersen, *ibid.* **74**, 125120 (2006).
[24] M. Imada and T. Kashima, J. Phys. Soc. Jpn. **69**, 2723 (2000); T. Kashima and M. Imada, *ibid.* **70**, 2287 (2001)
[25] For variational Monte Carlo studies, see W. L. McMillan, Phys. Rev. **138**, A442 (1965); D. Ceperley, G. V. Chester, and M. H. Kalos, Phys. Rev. B **16**, 3081 (1977); H. Yokoyama and H. Shiba, J. Phys. Soc. Jpn. **56**, 1490 (1987); as applications of a quantum Monte Carlo method to lattice Hubbard models, see R. Blankenbecler, D. J. Scalapino, and R. L. Sugar, Phys. Rev. D **24**, 2278 (1981); S. R. White, D. J. Scalapino, R. L. Sugar, E. Y. Loh, J. E. Gubernatis, and R. T. Scalettar, Phys. Rev. B **40**, 506 (1989); M. Imada and Y. Hatsugai, J. Phys. Soc. Jpn. **58**, 3752 (1989); N. Furukawa and M. Imada, *ibid.* **61**, 3331 (1992).
[26] I. Schnell, G. Czycholl, and R. C. Albers, Phys. Rev. B **65**, 075103 (2002); **68**, 245102 (2003).
[27] M. Posternak, A. Baldereschi, S. Massidda, and N. Marzari, Phys. Rev. B **65**, 184422 (2002).
[28] P. H. Dederichs, S. Blugel, R. Zeller, and H. Akai, Phys. Rev. Lett. **53**, 2512 (1984); M. R. Norman and A. J. Freeman, Phys. Rev. B **33**, 8896 (1986); O. Gunnarsson, O. K. Andersen, O. Jepsen, and J. Zaanen, *ibid.* **39**, 1708 (1989); M. S. Hybertsen, M. Schlüter, and N. E. Christensen, *ibid.* **39**, 9028 (1989); A. K. McMahan, J. F. Annett, and R. M. Martin, *ibid.* **42**, 6268 (1990); M. M. Steiner, R. C. Albers, and L. J. Sham, *ibid.* **45**, 13272 (1992); I. V. Solovyev and P. H. Dederichs, *ibid.* **49**, 6736 (1994); I. V. Solovyev, P. H. Dederichs, and V. I. Anisimov, *ibid.* **50**, 16861 (1994); As a constrained calculation for complex molecules, see Q. Wu and T. VanVoorhis, Phys. Rev. A **72**, 024502 (2005).
[29] For another approach for obtaining the on-site interaction parameter, see M. Springer and F. Aryasetiawan, Phys. Rev. B **57**, 4364 (1998); A. Yamasaki and T. Fujiwara, J. Phys. Soc. Jpn. **72**, 607 (2003).
[30] P. Lautenschlager, M. Garriga, S. Logothetidis, and M. Cardona, Phys. Rev. B **35**, 9174 (1987).
[31] D. E. Aspnes and A. A. Studna, Phys. Rev. B **27**, 985 (1983).
[32] J. Yamauchi, M. Tsukada, S. Watanabe, and O. Sugino, Phys. Rev. B **54**, 5586 (1996).

[33] J. P. Perdew, K. Burke, and M. Ernzerhof, Phys. Rev. Lett. **77**, 3865 (1996).
[34] N. Troullier and J. L. Martins, Phys. Rev. B **43**, 1993 (1991).
[35] L. Kleinman and D. M. Bylander, Phys. Rev. Lett. **48**, 1425 (1982).
[36] J. A. Pople, D. P. Santry, and G. A. Segal, J. Chem. Phys. **43**, S129 (1965); J. A. Pople and G. A. Segal, *ibid.* **43**, S136 (1965); J. A. Pople and G. A. Segal, *ibid.* **44**, 3289 (1966); J. A. Pople and D. L. Beveridge, *Approximate Molecular Orbital Theory* (McGrawHill, New York, London, 1970).
[37] D. Weider and U. Scherz, Phys. Rev. B **32**, 5273 (1985); O. Rotthaus, O. Jarjayes, F. Thomas, C. Philouze, C. P. Del Valle, E. Saint-Aman, and J.-L. Pierre, Chem.-Eur. J. **12**, 2293 (2006).
[38] Q. Xie, G. Archontis, and S. S. Skourtis, Chem. Phys. Lett. **312**, 237 (1999).
[39] T. R. Prytkova, D. N. Beratan, and S. S. Skourtis, Proc. Natl. Acad. Sci. U.S.A. **102**, 16128 (2007).
[40] J. B. McKitterick, Phys. Rev. B **28**, 7384 (1983).
[41] For the detail of the hopping-cutoff treatment, see K. Held, I. A. Nekrasov, G. Keller, V. Eyert, N. Blumer, A. K. McMahan, R. T. Scalettar, Th. Pruschke, V. I. Anisimov, and D. Vollhardt, Phys. Status Solidi B **243**, 2599 (2006).
[42] Our constrained calculations were performed for a $3\times3\times3$ fcc supercell containing 54 atoms, with $7\times7\times7$ k-point sampling. It was found that the sizes of the supercell and sampling k points are sufficient for obtaining converged interaction parameters.
[43] K. Nakamura, R. Arita, Y. Yoshimoto, and S. Tsuneyuki, Phys. Rev. B **74**, 235113 (2006).
[44] A. Ikawa, J. Phys. Soc. Jpn. **63**, 1986 (1994).
[45] D. L. Johnson, Phys. Rev. B **9**, 4475 (1974); S. G. Louie, J. R. Chelikowsky, and M. L. Cohen, Phys. Rev. Lett. **34**, 155 (1975).
[46] X. Wang, J. R. Yates, I. Souza, and D. Vanderbilt, Phys. Rev. B **74**, 195118 (2006).
[47] R. DelSole and R. Girlanda, Phys. Rev. B **48**, 11789 (1993); O. Pulci, G. Onida, A. I. Shkrebtii, R. DelSole, and B. Adolph, *ibid.* **55**, 6685 (1997).
[48] For a recent GW study for complicated systems such as liquid water or silicon nanowire, including optical absorption calculations, see V. Garbuio, M. Cascella, L. Reining, R. DelSole, and O. Pulci, Phys. Rev. Lett. **97**, 137402 (2006); L. Yang, C. D. Spataru, S. G. Louie, and M. Y. Chou, Phys. Rev. B **75**, 201304(R) (2007).